Inorganic Chemistry

Article

pubs.acs.org/IC

Substituent-Dependent Optical and Electrochemical Properties of Triarylformazanate Boron Difluoride Complexes

Stephanie M. Barbon, Jacquelyn T. Price, Pauline A. Reinkeluers, and Joe B. Gilroy*

Department of Chemistry and the Centre for Advanced Materials and Biomaterials Research (CAMBR), The University of Western Ontario, 1151 Richmond St. N., London, Ontario Canada, N6A 5B7

Supporting Information

ABSTRACT: The straightforward synthesis and detailed characterization of nine substituted triarylformazanate boron difluoride complexes is reported. The effect of electron-donating (*p*-anisole) and electron-withdrawing (*p*-benzonitrile) substituents on optical and electrochemical properties, relative to phenyl substituents, was studied at two different positions within the formazanate ligand framework. Each of the BF_2 complexes was characterized by ^{1}H, ^{13}C, ^{11}B, and ^{19}F NMR spectroscopy, cyclic voltammetry, infrared spectroscopy, UV−vis absorption and emission spectroscopy, mass spectrometry, and elemental analysis. Select examples were studied by X-ray crystallography, revealing highly delocalized structures in the solid state. The complexes were reversibly reduced in two steps electrochemically to their radical anion and dianion forms. The complexes also exhibited substituent-dependent absorption and emission properties, accompanied by significant Stokes shifts, with the aryl substituents at the 1,5-positions of the formazanate backbone having a greater influence on these properties than aryl substituents at the 3-position. Breaking the symmetry in three different complexes resulted in a modest increase in emission intensity relative to that of symmetrically substituted derivatives.

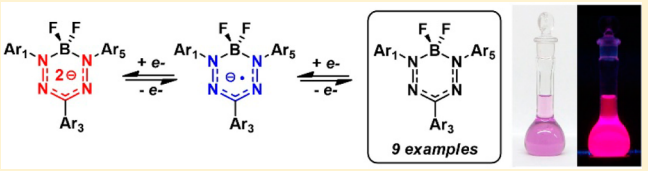

INTRODUCTION

Boron difluoride (BF_2) complexes of chelating *N*-donor ligands have been extensively studied over the past 20 years[1] as they tend to have interesting and useful properties that are tunable through structural modification, including high molar absorptivities and fluorescence quantum yields and unusual redox behavior. A wide range of chelating *N*-donor ligands have been studied as the backbone of these BF_2 complexes, including dipyrrins,[2] *β*-diketiminates,[3] anilido-pyridines,[4] anilido-imines,[5] pyridomethenes,[6] and indigo-*N*,*N*′-diarylamines,[7] resulting in complexes **1**−**6**. Complexes derived from dipyrrin ligands **1**, commonly known as BODIPYs, have been widely used in a number of applications due to their high quantum yields, although their syntheses can be challenging.[2,8] BF_2 complexes of *β*-diketiminates **2** are redox-active and exhibit high extinction coefficients, but have been shown to have low fluorescence quantum yields.[3] Piers' anilido-pyridine BF_2 complexes, **3**, have high quantum yields and exhibit large Stokes shifts,[4] as do related complexes based on anilido-imines **4**.[5] The large Stokes shifts are a key requirement for the potential use of BF_2 complexes as optical imaging agents. Pyridomethane BF_2 complexes **5** exhibit moderate quantum yields in solution and the solid state,[6] while those derived from indigo-*N*,*N*′-diarylamines, **6**, have rich redox chemistry and are emissive in the near-IR range.[7]

One set of chelating *N*-donor ligands that has not been widely studied in this context are formazanate ligands **7**,[9] which are derived from formazans **8**. Formazans have been used widely within the textile industry as dyes[10] and as colorimetric indicators of cell activity.[11] However, their behavior as ligands has only been explored intermittently over the past 75 years.[12] In the past decade, the Hicks group has reported a series of transition metal complexes of 3-cyanoformazanates and 3-nitroformazanates, including heteroleptic nickel complex **9** and iron and cobalt complexes **10a**,**b** derived from a tetradentate, trianionic 3-cyanoformazanate ligand.[12h] Tolman and co-workers have isolated copper(II) complexes of 3-nitroformazanates (for example, **11**) during studies designed to

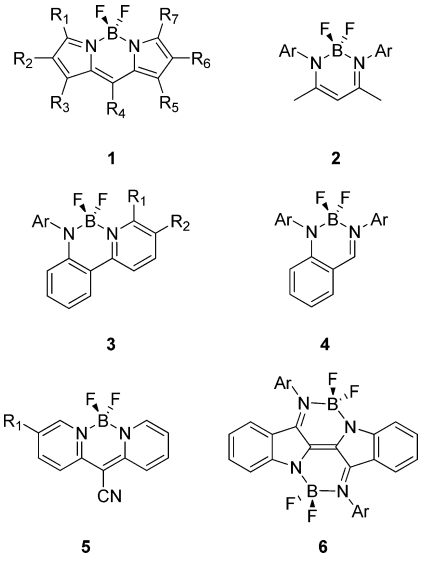

Received: July 16, 2014
Published: September 16, 2014

   dx.doi.org/10.1021/ic5016912 | *Inorg. Chem.* 2014, 53, 10585−10593

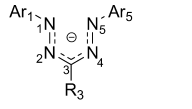

7

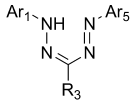

8

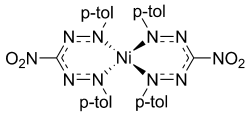

9

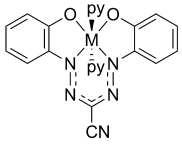

10a: M = Fe
10b: M = Co
py = pyridine

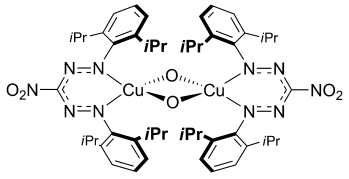

11

model oxygen activation processes prevalent in biological systems.[12i,j]

More recently, the Otten group has employed triarylformazans, for example, **12a**, for the synthesis of homoleptic zinc complexes, for example, **13**, and demonstrated the utility of formazanate ligands as electron acceptors.[13] While this manuscript was being prepared, a report describing the use of these zinc complexes as starting materials for the production of formazanate BF_2 complexes, for example, **14a**, via a transmetalation reaction was published (Scheme 1).[14] Herein, we extend a synthetic pathway previously used to produce a series of 3-cyanoformazanate BF_2 complexes,[15] to afford a series of triarylformazanate BF_2 complexes. Through judicious structural variation, we study the effect of substituents on their optical and electronic properties.

RESULTS

Synthesis. Formazans **12a–i** were prepared according to a previously published procedure[16] and exhibited a characteristic NH shift between 14 and 16 ppm in their ^{1}H NMR spectra (Supporting Information, Figures S1–S6). Triarylformazanate BF_2 complexes **14a–i** were synthesized from their parent formazans by heating at reflux in a toluene solution containing excess boron trifluoride diethyl etherate and triethylamine for 16 h (Scheme 2, Table 1). Purified yields ranged from 55 to 92%, with the exception of **14b**, which was isolated in 16% yield due to difficulties during purification.[17]

The incorporation of the $[BF_2]^+$ fragment into the formazanate framework was accompanied by a color change from dark red to purple. This structural change was also

Scheme 2. Synthesis of BF_2 Formazanate Complexes 14a–i

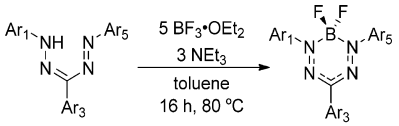

12a-i **14a-i**

Table 1. List of Substituents for Formazans 12a–i and BF_2 Formazanate Complexes 14a–i[a]

	Ar_1	Ar_5	Ar_3
a	C_6H_5	C_6H_5	*p*-C_6H_4–CH_3
b	*p*-C_6H_4–CN	*p*-C_6H_4–CN	*p*-C_6H_4–CH_3
c	*p*-C_6H_4–OMe	*p*-C_6H_4–OMe	*p*-C_6H_4–CH_3
d	*p*-C_6H_4–CH_3	*p*-C_6H_4–CH_3	C_6H_5
e	*p*-C_6H_4–CH_3	*p*-C_6H_4–CH_3	*p*-C_6H_4–CN
f	*p*-C_6H_4–CH_3	*p*-C_6H_4–CH_3	*p*-C_6H_4–OMe
g	*p*-C_6H_4–CN	*p*-C_6H_4–OMe	*p*-C_6H_4–CH_3
h	*p*-C_6H_4–CH_3	*p*-C_6H_4–CN	*p*-C_6H_4–OMe
i	*p*-C_6H_4–OMe	*p*-C_6H_4–CH_3	*p*-C_6H_4–CN

[a] *p*-C_6H_4–CH_3 substituents were chosen as "placeholders" throughout this study, as their presence simplified NMR spectra and facilitated purification by crystallization.

observed in the ^{1}H NMR spectra of **14a–i**, as the respective NH signals disappeared (Figure 1 and Supporting Information, Figures S7–S22). The BF_2 formazanate complexes were also characterized by ^{11}B and ^{19}F NMR spectroscopy, where diagnostic 1:2:1 triplets in the ^{11}B NMR spectra between −0.5 and −0.7 ppm, and 1:1:1:1 quartets in the ^{19}F NMR spectra between −142.9 and −145.8 ppm were observed. Further analysis by ^{13}C NMR spectroscopy, mass spectrometry, IR spectroscopy, and elemental analysis confirmed the proposed structures of complexes **14a–i**.

X-ray Crystallography. Slow evaporation of concentrated dichloromethane solutions of **14d–f** yielded single crystals suitable for X-ray diffraction analysis. The solid-state structures of **14d–f** (Figure 2 and Table 2) confirm the presence of four-coordinate boron, bound to the formazanate backbone through two nitrogen atoms. In each structure, the formazanate backbone is delocalized, as the C–N and N–N bonds are approximately halfway between a single and double bond of the respective atoms involved.[18] Each boron center exists in a distorted tetrahedral geometry, and the boron atom is slightly displaced from the N1–N2–N3–N4 plane, by 0.022 Å in **14d** and 0.290 Å in **14e**. The solid-state structure of **14f** is dissimilar to those determined for **14d** and **14e** and is shaped like a "dragonfly," with the boron atom displaced from the N1–N2–N3–N4 plane by 0.538 Å in **14f** in a boat-like conformation. A similar structure was observed for an electron-rich 1,5-*p*-anisole-3-cyanoformazanate BF_2 complex where

Scheme 1. Otten's Synthesis of Homoleptic Zinc Formazanate Complex 13 And Boron Difluoride Formazanate Complex 14a[13,14]

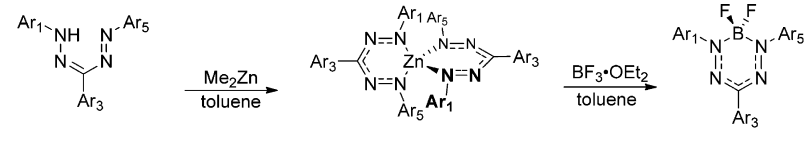

12a: Ar_1 = Ar_3 = Ph, Ar_5 = *p*-tol **13** **14a**

dx.doi.org/10.1021/ic5016912 | Inorg. Chem. 2014, 53, 10585–10593

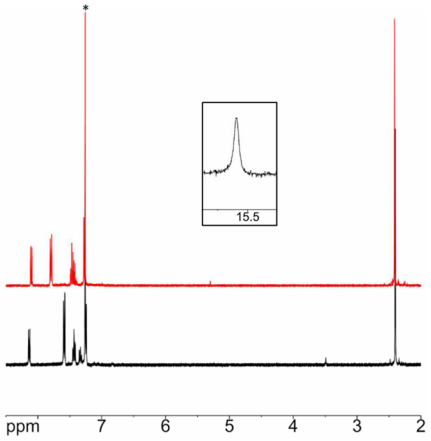

Figure 1. ^{1}H NMR spectra of formazan **12d** (black) and BF_2 complex **14d** (red) in $CDCl_3$. The asterisk denotes residual solvent signals. (inset) The NH signal for **12d**.

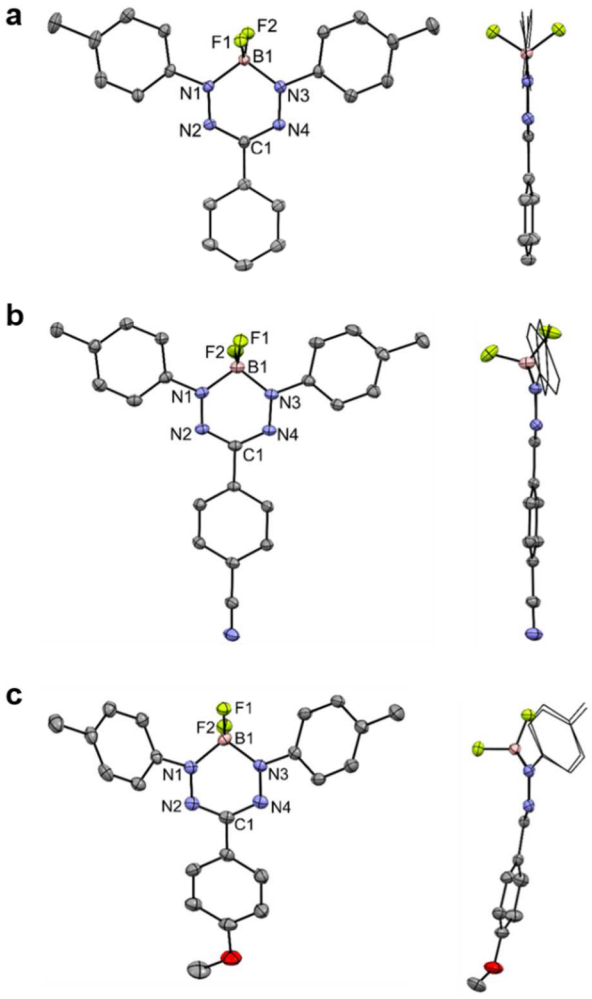

Figure 2. Solid-state structures of (a) top view (left) and side view (right) for **14d**, (b) top view (left) and side view (right) for **14e**, (c) top view (left) and side view (right) for **14f**. Thermal ellipsoids are shown at 50% probability, and hydrogen atoms are removed for clarity.

planar and boat conformations were shown to differ by ca. 5 kJ mol^{-1}.[15] The *N*-aryl substituents are twisted by 7° and 5° in **14d** and 8° and 25° in **14e**, with respect to the N1−N2−N3−N4 plane. The solid-state structure of **14f** exhibits much larger twisting of the *N*-aryl substituents, relative to the N1−N2−N3−N4 plane, with twisting of 43° and 50° as was seen in its 3-cyanoformazanate analog.[15] The structures of **14d−f** are similar to the structure of complex **14a** reported previously.[14]

Absorption and Emission Spectroscopy. The optical properties of BF_2 complexes **14a−i** were explored in three different solvents using UV−vis absorption and emission spectroscopy (Figure 3, Table 3, and Supporting Information, Figures S23−S33). First we will discuss the spectral trends observed upon variation of the 1,5-substitutents (phenyl, *p*-benzonitrile, *p*-anisole) in complexes **14a−c**. Each complex was highly absorbing between 450 and 600 nm, with wavelengths of maximum absorption (λ_{max}) in toluene of 523 nm (ε = 22 400 M^{-1} cm^{-1}) for **14a**, 550 nm (ε = 20 500 M^{-1} cm^{-1}) for **14b**, and 552 nm (ε = 28 200 M^{-1} cm^{-1}) for **14c**. Because of the electron-donating nature of the 1,5-(*p*-anisole) substituents in **14c**, the λ_{max} of **14c** was red-shifted by ca. 25 nm with respect to the phenyl-substituted analog **14a**. The λ_{max} of the *p*-benzonitrile-substituted derivative, **14b**, was also red-shifted relative to **14a**. Although this observation may seem counter-intuitive, the same trend was observed for monosubstituted benzenes (Supporting Information, Figure S26). Each complex in the series **14a−c** was shown to be emissive, with wavelengths of maximum emission (λ_{em}) of 639, 674, and 686 nm, respectively, in toluene. The trends observed for the emission spectra mirrored those observed for the absorption spectra. The observed Stokes shifts (ν_{ST}) were significant, ν_{ST} = 3470 cm^{-1} (**14a**), 3345 cm^{-1} (**14b**), and 3540 cm^{-1} (**14c**) in toluene, and quantum yields (Φ) were calculated to be between 0.5% and 5.0% and were highest for electron-donating *p*-anisole-substitued **14c**. Under identical conditions similarly substituted 3-cyanoformazanate BF_2 complexes exhibited quantum yields between 14% and 77% and Stokes shifts ranging from 2239 to 2855 cm^{-1}.[15]

Complexes **14d−f** were studied to assess the influence of the same series of aryl substituents at the 3-position of the formazanate framework. Similar to compounds **14a−c**, all three complexes were highly absorbing between 450 and 600 nm, with high molar absorptivities at their respective λ_{max} in toluene [**14d**: λ_{max} = 524 nm (ε = 30 300 M^{-1} cm^{-1}); **14e**: λ_{max} = 525 nm (ε = 25 300 M^{-1} cm^{-1}); **14f**: λ_{max} = 544 nm (ε = 25 800 M^{-1} cm^{-1})]. Again, the λ_{max} for the 3-(*p*-anisole)-substituted derivative (**14f**), was significantly red-shifted with respect to the phenyl-substituted complex (**14d**), but unlike the **14a−c** series, a red shift in λ_{max} was not observed for complex **14e** (Ar_3 = *p*-C_6H_4−CN). The observed trend was similar for the emission spectra of complexes **14d−f**, where the λ_{em} for **14f** (Ar_3 = *p*-C_6H_4−OMe, λ_{em} = 669 nm) was red-shifted relative to the λ_{em} for **14d** (Ar_3 = C_6H_5, λ_{em} = 640 nm). However, a blue shift in λ_{em} for the electron-withdrawing *p*-benzonitrile-substituted complex **14e** (λ_{em} = 634 nm) was observed relative to **14d**. The Stokes shifts for complexes **14d−f** were again substantial (3275−3460 cm^{-1}), and the calculated quantum yields ranged from 0.5 to 2.0%, with the 3-(*p*-benzonitrile)-substituted BF_2 complex (**14e**) exhibiting the highest quantum yield in toluene.

Finally, we studied the optical properties of asymmetrically substituted complexes **14g−i**, which contain *p*-anisole, *p*-benzonitrile, and *p*-tolyl substituents in three different arrangements. All three systems absorbed visible light between 450 and 650 nm and had λ_{max} values of 561 nm (ε = 24 400 M^{-1} cm^{-1}), 560 nm (ε = 21 500 M^{-1} cm^{-1}), and 541 nm (ε = 25 100 M^{-1} cm^{-1}), respectively. In toluene, their λ_{em} values were 666 nm (**14g**), 672 nm (**14h**), and 651 nm (**14i**). These complexes also

dx.doi.org/10.1021/ic5016912 | *Inorg. Chem.* 2014, 53, 10585−10593

Table 2. Selected Bond Lengths (Å) and Angles (deg) for BF_2 Formazanate Complexes 14d–f, Determined by X-ray Diffraction

	14d	14e	14f
N1–N2, N3–N4	1.3117(18), 1.3094(18)	1.3012(17), 1.3085(17)	1.315(3), 1.315(3)
C1–N2, C1–N4	1.339(2), 1.346(2)	1.3431(19), 1.340(2)	1.344(3), 1.338(3)
N1–B1, N3–B1	1.561(2), 1.561(2)	1.560(2), 1.576(2)	1.551(4), 1.556(4)
N1–N2–C1, N3–N4–C1	118.84(13), 118.78(13)	118.24(12), 118.57(12)	117.2(2), 117.3(2)
N2–C1–N4	126.66(14)	126.83(13)	124.6(2)
N1–B1–N3	106.28(12)	105.17(12)	101.68(19)
boron displacement[a]	0.022	0.290	0.538
dihedral angles[b]	7.20, 5.48, 6.38	25.52, 7.78, 6.22	50.26, 43.08, 17.20

[a]Distance between B1 and N1–N2–N3–N4 plane. [b]Angles between the plane defined by the N1, N3, and C1 aryl substituents and the N1–N2–N3–N4 plane.

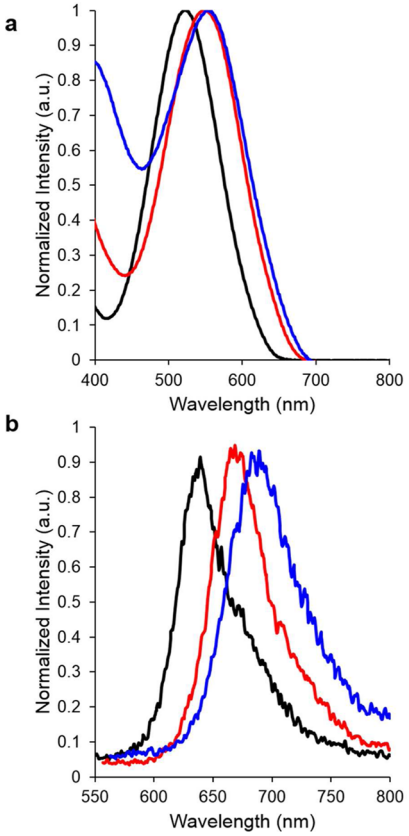

Figure 3. UV–vis absorption spectra (a) and emission spectra (b) of **14a** (black), **14b** (red), and **14c** (blue), recorded for 10^{-5} M degassed toluene solutions.

exhibited significant Stokes shifts between 2810 and 3125 cm^{-1} and calculated quantum yields of 8.7% for **14g**, 5.3% for **14h**, and 9.8% for **14i**.

Cyclic Voltammetry. The substituent effects for complexes **14a–i** were studied by cyclic voltammetry (CV). Each complex exhibited two ligand-centered reversible (or quasi-reversible) one-electron reduction waves corresponding to the production of their radical anion (**15**) and dianion (**16**) forms (Scheme 3, Figure 4, Table 4, and Supporting Information, Figures S34 and S35). Most of the complexes studied also exhibited irreversible oxidation events in their CVs within the electrochemical window of acetonitrile (Supporting Information, Figures S36–S38).

Again we begin by discussing 1,5-substituted complexes **14a–c**. Phenyl-substituted complex **14a** was reversibly reduced at E^{o}_{red1} = −830 mV and E^{o}_{red2} = −1870 mV. The introduction of electron-withdrawing *p*-benzonitrile substituents in complex **14b** substantially decreased the potential required for reduction to E^{o}_{red1} = −500 mV and E^{o}_{red2} = −1470 mV. Electron-rich, *p*-anisole-substituted complex **14c** was more difficult to reduce than **14a,b**, with reduction waves observed at E^{o}_{red1} = −970 mV and E^{o}_{red2} = −1940 mV. All three complexes have reduction waves separated (ΔE) by approximately 1000 mV and were significantly more difficult to reduce than their 3-cyanoformazanate analogues.[15]

The trends observed for the 3-substituted formazanate complexes **14d–f** were not obvious. The phenyl-substituted derivative was reduced at potentials of E^{o}_{red1} = −920 mV and E^{o}_{red2} = −1930 mV, while *p*-benzonitrile-substituted complex **14e** was easier to reduce (E^{o}_{red1} = −830 mV and E^{o}_{red2} = −1920 mV). Unexpectedly, *p*-anisole-substituted complex **14f** was also slightly easier to reduce than **14d** at E^{o}_{red1} = −900 mV and E^{o}_{red2} = −1890 mV. Similar to complexes **14a–c**, the ΔE values for **14d–f** were ca. 1000 mV.

For the series of asymmetrically substituted BF_2 complexes **14g–i**, the 1,5-substituents had the most significant effect on their electrochemical reduction. Complex **14g**, bearing *p*-anisole and *p*-benzonitrile substituents at the 1,5-positions, was reversibly reduced at E^{o}_{red1} = −720 mV and E^{o}_{red2} = −1740 mV. Interchanging the electron-donating *p*-anisole substituent with a weakly donating *p*-tolyl group in complex **14h** decreased the reduction potentials by ca. 30 mV to E^{o}_{red1} = −690 mV and E^{o}_{red2} = −1720 mV. Complex **14i** has two donating *N*-substituents (*p*-anisole and *p*-tolyl), and thus was the most difficult to reduce, at E^{o}_{red1} = −860 mV and E^{o}_{red2} = −1940 mV. The ΔE values for these complexes were 1020 mV for **14g**, 1030 mV for **14h**, and 1080 mV for **14i**. Interestingly, **14e** and **14i** exhibit a third reversible reduction wave within the solvent window, perhaps due to the formation of radical trianions (Supporting Information, Figures S37 and S38).

DISCUSSION

Through inspection of the electrochemical and optical spectroscopy data collected for complexes **14a–f**, it is clear that the 1,5-substituents have a more pronounced effect on the properties observed. For the series **14a–c**, predictable trends in reduction potentials based on the electron donating/withdrawing character of the *N*-aryl substituents were observed, including a shift of ca. 500 mV in the reduction potentials (E^{o}_{red1} and E^{o}_{red2}) upon switching from *p*-benzonitrile to *p*-anisole 1,5-substituents. For **14d–f**, the observed trend is not easily rationalized, as the electron-rich 3-(*p*-anisole) derivative was easier to reduce than the 3-phenyl analogue. Similarly, the absorption and emission properties of **14a–f** were much more sensitive to the 1,5-substituents than the 3-substituents. These

dx.doi.org/10.1021/ic5016912 | Inorg. Chem. 2014, 53, 10585–10593

Table 3. Optical Properties of BF_2 Formazanate Complexes 14a–i

compound	solvent	λ_{max} (nm)	ε (M^{-1} cm^{-1})	λ_{em} (nm)	Φ (%)[a]	ν_{ST} (cm^{-1})	ν_{ST} (nm)
14a	THF	517	21 700	641	0.5	3740	124
	dichloromethane	518	24 700	641	0.8	3705	123
	toluene	523	22 400	639	0.7	3470	116
14b	THF	541	22 800	673	1.5	3625	132
	dichloromethane	545	24 500	678	0.9	3600	133
	toluene	550	20 500	674	2.1	3345	124
14c	THF	545	22 300	692	1.5	3900	147
	dichloromethane	544	29 300	690	2.4	3890	146
	toluene	552	28 200	686	5.0	3540	134
14d	THF	520	29 300	641	0.6	3630	121
	dichloromethane	520	36 600	640	0.5	3610	120
	toluene	524	30 300	640	0.9	3460	116
14e	THF	521	33 800	631	0.9	3350	110
	dichloromethane	521	36 600	631	0.7	3350	110
	toluene	525	25 300	634	2.0	3275	109
14f	THF	539	24 600	674	1.1	3715	135
	dichloromethane	539	25 200	673	1.1	3695	134
	toluene	544	25 800	669	1.4	3435	125
14g	THF	552	30 100	667	5.4	3125	115
	dichloromethane	553	27 500	666	6.2	3070	113
	toluene	561	24 400	666	8.7	2810	105
14h	THF	553	22 500	674	4.1	3245	121
	dichloromethane	553	24 500	676	3.8	3290	123
	toluene	560	21 500	672	5.3	2975	112
14i	THF	535	32 500	651	6.4	3330	116
	dichloromethane	534	33 900	651	5.8	3365	117
	toluene	541	25 100	651	9.8	3125	110

[a]Quantum yields were measured according to published protocols[19] using ruthenium tris(bipyridine) hexafluorophosphate as a relative standard[20] and corrected for wavelength-dependent detector sensitivity (Supporting Information, Figure S33).

Scheme 3. Stepwise Reduction of Triarylformazanate BF_2 Complexes

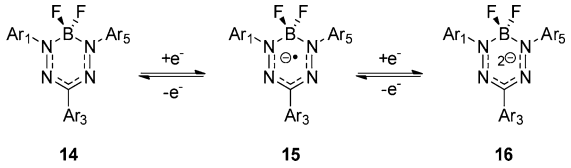

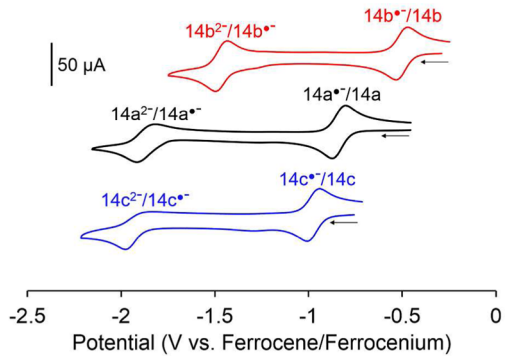

Figure 4. Cyclic voltammograms of **14a** (black), **14b** (red), and **14c** (blue) recorded at 250 mV s^{-1} in 1 mM acetonitrile solutions containing 0.1 M tetrabutylammonium hexafluorophosphate as supporting electrolyte.

Table 4. Electrochemical Data (mV vs Fc/Fc^+) for BF_2 Formazanate Complexes 14a–i

	E^{o}_{red1}[a] (mV)	E^{o}_{red2}[a] (mV)	ΔE (mV)
14a	−840	−1870	1030
14b	−500	−1470	970
14c	−970	−1940	970
14d	−920	−1930	1010
14e	−830	−1920	1090
14f	−900	−1890	990
14g	−720	−1740	1020
14h	−690	−1720	1030
14i	−860	−1940	1080

[a]Cyclic voltammetry experiments were conducted in acetonitrile containing 1 mM analyte and 0.1 M tetrabutylammonium hexafluorophosphate as supporting electrolyte at a scan rate of 250 mV s^{-1}. All voltammograms were referenced internally against the ferrocene/ferrocenium redox couple.

trends are similar to those observed for Kuhn-type verdazyls **17** and 6-oxoverdazyls **18**, where the singly occupied molecular orbital (π-SOMO) is centered on the four nitrogen atoms and contains very little electron density at the 3-position of the heterocyclic ring due to the presence of a nodal plane.[16b,21] The LUMOs of a series of 3-cyanoformazanate BF_2 complexes were recently shown to possess very similar features,[15] and the LUMOs of the triarylformazanate BF_2 complexes described in this paper are not expected to differ significantly.

Breaking the symmetry in complexes **14g–i** did not result in significant changes in electrochemical or absorption properties relative to symmetrically substituted analogs **14a–f**. However, a modest enhancement in quantum yields was observed for all three substituent configurations. This enhancement of emission intensity is consistent with trends observed for asymmetrically

dx.doi.org/10.1021/ic5016912 | Inorg. Chem. 2014, 53, 10585–10593

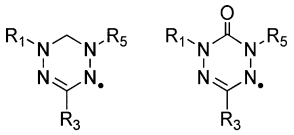

17 18

substituted BODIPYs[22] and other BF_2 complexes of *N*-donor ligands.[23] For all of the complexes studied (**14a−i**), the emission intensities, and thus quantum yields, were higher in toluene than they were in THF or in dichloromethane. This effect may arise due to the stabilization of polar excited states, by polar solvents, potentially allowing for competing deactivation pathways to operate.[24]

The Stokes shifts observed for compounds **14a−i** range from 2810 to 3900 cm^{-1} (105−147 nm). These values are larger than those observed for BF_2 complexes of *N*-donor ligands such as dipyrrins (200−1859 cm^{-1})[25] and pyridomethenes (238−1031 cm^{-1})[6] and are smaller than those observed for *β*-diketiminates (3741−6074 cm^{-1})[3c] and anilido-pyridines (3877−5148 cm^{-1}).[4] The origin of this fundamental property of formazanate boron difluoride complexes **14a−i** will be the subject of future work.

CONCLUSIONS

In conclusion, we have demonstrated a straightforward synthetic route to a series of nine triarylformazanate boron difluoride complexes allowing for studies of their substituent-dependent properties to be conducted. We have shown that the properties of these complexes, including their wavelengths of maximum absorption and emission, quantum yields, and electrochemical properties can be tuned by the introduction of electron-donating (*p*-anisole) or electron-withdrawing (*p*-benzonitrile) aryl substituents at the formazanate ligand backbone. Changes in the properties observed were most dramatic when 1,5-substituents were varied compared to similar structural variations at the 3-position of the formazanate backbone. Modest enhancements in emission intensity were observed for asymmetrically substituted complexes, which exhibited quantum yields close to 10%. Our future work in this area will focus on the introduction of polymerizable functional groups to triarylformazanate BF_2 complexes toward redox-active functional polymers.

EXPERIMENTAL SECTION

General Considerations. All reactions and manipulations were carried out under a nitrogen atmosphere using standard Schlenk techniques unless otherwise stated. Solvents were obtained from Caledon Laboratories, dried using an Innovative Technologies Inc. solvent purification system, collected under vacuum, and stored under a nitrogen atmosphere over 4 Å molecular sieves. All reagents were purchased from Sigma-Aldrich or Alfa Aesar and used as received. Formazans **12a−i** were synthesized according to previously published procedures, and the characterization data for **12a−f** were consistent with the same report.[16b]

NMR spectra were recorded on a 400 MHz (^{1}H: 399.8 MHz, ^{11}B: 128.3 MHz, ^{19}F: 376.1 MHz) or 600 MHz (^{1}H: 599.5 MHz, ^{13}C: 150.8 MHz) Varian INOVA instrument or a 400 MHz (^{13}C: 100.6 MHz) Varian Mercury Instrument. ^{1}H NMR spectra were referenced to residual $CHCl_3$ (7.27 ppm), and ^{13}C NMR spectra were referenced to $CDCl_3$ (77.2 ppm). ^{11}B spectra were referenced to $BF_3{\cdot}OEt_2$ at 0 ppm, and ^{19}F spectra were referenced to $CFCl_3$ at 0 ppm. Mass spectrometry data were recorded in positive-ion mode using a high-resolution Finnigan MAT 8200 spectrometer using electron impact ionization (EI). UV−vis spectra were recorded using a Cary 300 Scan instrument. Four separate concentrations were run for each sample, and molar extinction coefficients were determined from the slope of a plot of absorbance against concentration. Infrared spectra were recorded on a KBr disk using a Bruker Vector 33 FT-IR spectrometer. Emission spectra were obtained using a Photon Technology International QM-4 SE spectrofluorometer. Excitation wavelengths were chosen based on λ_{max} from the respective UV−vis absorption spectrum in the same solvent. Quantum yields were estimated relative to ruthenium tris(bipyridine) hexafluorophosphate by previously described methods and corrected for wavelength-dependent detector sensitivity (Supporting Information, Figure S33).[19,20] Elemental analyses (C, H, N) were carried out by Laboratoire d'Analyze Élémentaire de l'Université de Montréal, Montréal, QC, Canada.

Electrochemical Methods. Cyclic voltammetry experiments were performed with a Bioanalytical Systems Inc. (BASi) Epsilon potentiostat and analyzed using BASi Epsilon software. Electrochemical cells consisted of a three-electrode setup including a glassy carbon working electrode, platinum wire counter electrode, and silver wire pseudoreference electrode. Experiments were run at scan rates of 250 mV s^{-1} in degassed acetonitrile solutions of the analyte (∼1 mM) and supporting electrolyte (0.1 M tetrabutylammonium hexafluorophosphate). Cyclic voltammograms were referenced against an internal standard (∼1 mM ferrocene) and corrected for internal cell resistance using the BASi Epsilon software.

X-ray Crystallography Details. Single crystals of complexes **14d−f** suitable for X-ray diffraction studies were grown by slow evaporation of a concentrated solution of each compound in dichloromethane. The samples were mounted on a Mitegen polyimide micromount with a small amount of Paratone N oil. All X-ray measurements were made on a Bruker Kappa Axis Apex2 diffractometer at a temperature of 110 K. The data collection strategy included a number of ω and φ scans, collection strategy included a number of ω and ϕ scans. The frame integration was performed using SAINT.[26] The resulting raw data was scaled and absorption-corrected using a multiscan averaging of symmetry equivalent data using SADABS.[27] The structures were solved by direct methods using the XS program.[28] All non-hydrogen atoms were obtained from the initial solution. The hydrogen atoms were introduced at idealized positions and were allowed to refine isotropically. The structural model was fit to the data using full matrix least-squares based on F^2. The calculated structure factors included corrections for anomalous dispersion from the usual tabulation. The structure was refined using SHELXL-2014 from the SHELX suite of programs.[29] For complex **14f**, a fractional dichloromethane solvent was present, which could not be modeled reliably, so it was treated with the squeeze procedure in Platon.[30] See Table 5 for additional crystallographic data.

Representative Procedure: Formazan 12g (Ar_1 = *p*-C_6H_4−CN, Ar_5 = *p*-C_6H_4−OMe, Ar_3 = *p*-C_6H_4−CH_3). 4-cyanophenyl hydrazine hydrochloride (1.50 g, 8.80 mmol) was dissolved in ethanol (15 mL) with triethylamine (1.60 g, 2.21 mL, 15.8 mmol). *p*-Tolualdehyde (1.06 g, 1.04 mL, 8.80 mmol) was then added, and the solution was allowed to stir for 10 min. After this time, a light yellow precipitate had formed. Dichloromethane (50 mL) and water (50 mL) were added to form a biphasic reaction mixture. Sodium carbonate (3.17 g, 29.9 mmol) and tetrabutyl ammonium bromide (0.28 g, 0.88 mmol) were added, and the mixture was cooled in an ice bath to 0 °C. In a separate flask, *p*-anisidine (1.11 g, 9.00 mmol) and concentrated hydrochloric acid (3.6 mL, 43.2 mmol) were mixed in water (20 mL) and cooled in an ice bath. A cooled solution of sodium nitrite (0.69 g, 10 mmol) was added slowly to the aniline solution. This mixture was left to stir at 0 °C for 30 min, after which time it was added dropwise to the biphasic reaction mixture described above over 10 min. The resulting solution was stirred for 18 h, gradually turning dark red over this time. The dark red organic fraction was then washed with deionized water (3 × 50 mL), dried over $MgSO_4$, gravity filtered, and concentrated *in vacuo*. The resulting residue was purified by flash chromatography (dichloromethane, neutral alumina) to yield formazan **12g** as a dark red microcrystalline solid. Yield = 2.40 g, 74%. mp = 154−156 °C. ^{1}H NMR (599.5 MHz, $CDCl_3$) δ 14.26 (s, 1H, NH), 7.96 (d, $^3J_{HH}$ = 8 Hz, 2H, aryl C*H*), 7.93 (d, $^3J_{HH}$ = 9 Hz, 2H, aryl C*H*), 7.60 (d, $^3J_{HH}$ = 8

dx.doi.org/10.1021/ic5016912 | *Inorg. Chem.* 2014, 53, 10585−10593

Table 5. X-ray Diffraction Data Collection and Refinement Details for Complexes 14d–f

	14d	14e	14f
chemical formula	$C_{21}H_{19}BF_2N_4$	$C_{22}H_{18}BF_2N_5$	$C_{22}H_{21}BF_2N_4O$
FW (g/mol)	376.21	401.22	406.24
crystal habit	red plate	green rectangular	red needle
crystal system	monoclinic	monoclinic	triclinic
space group	$P2_1/n$	$P2_1/c$	$P\bar{1}$
T (K)	113(2)	110	110
λ (Å)	0.71073	0.71073	0.71073
a (Å)	9.7298(10)	16.818(7)	10.362(6)
b (Å)	18.713(2)	16.188(5)	28.120(17)
c (Å)	10.3804(12)	7.257(3)	28.16(2)
α (deg)	90	90	117.075(13)
β (deg)	97.825(6)	99.220(18)	96.626(17)
γ (deg)	90	90	98.667(16)
V (Å^3)	1872.4(4)	1950.0(13)	7062(8)
Z	4	4	12
ρ (g/cm^3)	1.335	1.367	1.146
μ (cm^{-1})	0.094	0.097	0.083
R_1,[a] wR_2[b] [$I > 2\sigma$]	0.0711, 0.1511	0.0599, 0.1676	0.0669, 0.1625
R_1, wR_2 (all data)	0.2110, 0.2048	0.0826, 0.1835	0.1407, 0.1849
GOF[c]	0.977	1.035	1.122

[a] $R_1 = \Sigma(|F_o| - |F_c|)/\Sigma F_o$. [b] $wR_2 = [\Sigma(w(F_o^2 - F_c^2)^2)/\Sigma(wF_o^4)]^{1/2}$. [c] GOF = $[\Sigma(w(F_o^2 - F_c^2)^2)/(\text{No. of reflns.} - \text{No. of params.})]^{1/2}$.

Hz, 2H, aryl C*H*), 7.40 (d, $^3J_{HH}$ = 8 Hz, 2H, aryl C*H*), 7.26 (d, $^3J_{HH}$ =8 Hz, 2H, aryl C*H*), 7.06 (d, $^3J_{HH}$ = 9 Hz, 2H, aryl C*H*), 3.93 (s, 3H, OCH_3), 2.42 (s, 3H, CH_3). $^{13}C\{^1H\}$ NMR (100.6 MHz, $CDCl_3$): δ 163.4, 147.5, 146.9, 143.0, 138.6, 133.8, 133.7, 129.3, 126.7, 124.8, 119.7, 114.9, 114.7, 104.7, 55.9, 21.5. FT-IR (KBr): 3420 (s), 3067 (m), 2918 (m), 2841 (m), 2219 (m), 1603 (s), 1509 (s), 1257 (s), 1231 (m), 1143 (m) cm^{-1}. UV–vis (toluene): λ_{max} = 489 nm (ε = 28 300 M^{-1} cm^{-1}). Mass spectrometry (MS) (EI, +ve mode): exact mass calculated for $[C_{22}H_{19}N_5O]^+$: 369.15896; exact mass found: 369.15983; difference: +2.34 ppm. Anal. Calcd (%) for $C_{22}H_{19}N_5O$: C, 71.53; H, 5.18; N, 18.96. Found: C, 71.43; H, 5.00; N, 18.76.

Formazan 12h (Ar_1 = *p*-C_6H_4–CH_3, Ar_5 = *p*-C_6H_4–CN, Ar_3 = *p*-C_6H_4–OMe). From 12.6 mmol of hydrazine/aldehyde: Yield = 3.74 g, 80%. mp = 156–158 °C. ^{1}H NMR (599.5 MHz, $CDCl_3$) δ 14.37 (s, 1H, NH), 8.02 (d, $^3J_{HH}$ = 9 Hz, 2H, aryl C*H*), 7.82 (d, $^3J_{HH}$ = 8 Hz, 2H, aryl C*H*), 7.60 (d, $^3J_{HH}$ = 9 Hz, 2H, aryl C*H*), 7.38 (d, $^3J_{HH}$ = 9 Hz, 2H, aryl C*H*), 7.35 (d, $^3J_{HH}$ =8 Hz, 2H, aryl C*H*), 6.98 (d, $^3J_{HH}$ = 8 Hz, 2H, aryl C*H*), 3.88 (s, 3H, OCH_3), 2.47 (s, 3H, CH_3). $^{13}C\{^1H\}$ NMR (100.6 MHz, $CDCl_3$): δ 160.2, 150.4, 147.5, 143.3, 142.6, 133.7, 130.3, 129.1, 128.1, 122.6, 119.7, 114.9, 114.0, 104.9, 55.5, 21.8. FT-IR (KBr): 3421 (s), 3003 (m), 2935 (m), 2840 (m), 2219 (s), 1603 (s), 1508 (s), 1248 (s), 1228 (s), 1170 (s) cm^{-1}. UV–vis (toluene): λ_{max} = 501 nm (ε = 16 800 M^{-1} cm^{-1}). MS (EI, +ve mode): exact mass calculated for $[C_{22}H_{19}N_5O]^+$: 369.15896; exact mass found: 369.15923; difference: +0.72 ppm. Anal. Calcd (%) for $C_{22}H_{19}N_5O$: C, 71.53; H, 5.18; N, 18.96. Found: C, 71.95; H, 5.17; N, 18.23.

Formazan 12i (Ar_1 = *p*-C_6H_4–OMe, Ar_5 = *p*-C_6H_4–CH_3, Ar_3 = *p*-C_6H_4–CN). From 12.6 mmol of hydrazine/aldehyde: Yield = 3.34 g, 72%. mp = 179–181 °C. ^{1}H NMR (599.5 MHz, $CDCl_3$) δ 15.61 (s, 1H, NH), 8.19 (d, $^3J_{HH}$ = 8 Hz, 2H, aryl C*H*), 7.76 (d, $^3J_{HH}$ = 9 Hz, 2H, aryl C*H*), 7.66 (d, $^3J_{HH}$ = 8 Hz, 2H, aryl C*H*), 7.38 (d, $^3J_{HH}$ = 8 Hz, 2H, aryl C*H*), 7.20 (d, $^3J_{HH}$ = 8 Hz, 2H, aryl C*H*), 7.01 (d, $^3J_{HH}$ = 9 Hz, 2H, aryl C*H*), 3.90 (s, 3H, OCH_3), 2.37 (s, 3H, CH_3). $^{13}C\{^1H\}$ NMR (100.6 MHz, $CDCl_3$): δ 161.4, 144.6, 142.2, 142.2, 138.7, 135.6, 132.1, 130.1, 125.6, 122.6, 119.5, 116.6, 114.7, 110.0, 55.7, 21.1. FT-IR (KBr): 3411 (s), 3003 (m), 2918 (m) 2841 (m), 2222 (s), 1603 (s), 1499 (s), 1248 (s), 1189 (m), 1145 (m) cm^{-1}. UV–vis (toluene): λ_{max} = 506 nm (ε = 22 400 M^{-1} cm^{-1}). MS (EI, +ve mode): exact mass calculated for $[C_{22}H_{19}N_5O]^+$: 369.15896; exact mass found: 369.16019; difference: +3.34 ppm. Anal. Calcd (%) for $C_{22}H_{19}N_5O$: C, 71.53; H, 5.18; N, 18.96. Found: C, 71.63; H, 5.14; N, 18.78.

Representative Procedure: Formazanate BF_2 Complex 14a (Ar_1 = C_6H_5, Ar_5 = C_6H_5, Ar_3 = *p*-C_6H_4–CH_3). Formazan **12a** (1.00 g, 2.76 mmol) was dissolved in dry toluene (100 mL). Triethylamine (0.84 g, 1.2 mL, 8.3 mmol) was then added slowly, and the solution was allowed to stir for 10 min. Boron trifluoride diethyl etherate (1.96 g, 1.73 mL, 13.8 mmol) was then added, and the solution was heated at 80 °C for 18 h. The solution gradually turned from dark red to dark purple during this time. After the reaction was cooled to 20 °C, deionized water (10 mL) was added to quench any excess reactive boron-containing compounds. The purple toluene solution was then washed with deionized water (3 × 50 mL), dried over $MgSO_4$, gravity filtered, and concentrated *in vacuo*. The resulting residue was purified by flash chromatography (dichloromethane, neutral alumina) to yield the BF_2 complex as a dark purple microcrystalline solid. Yield = 0.69 g, 60%. ^{1}H NMR (599.5 MHz, $CDCl_3$) δ 8.01 (d, $^3J_{HH}$ = 8 Hz, 2H, aryl C*H*), 7.91 (d, $^3J_{HH}$ = 7 Hz, 4H, aryl C*H*), 7.47 (m, 6H, aryl C*H*), 7.30 (d, $^3J_{HH}$ = 8 Hz, 2H, aryl C*H*), 2.44 (s, 3H, CH_3). These data were consistent with those reported by Otten and co-workers.[14]

Formazanate BF_2 Complex 14b (Ar_1 = *p*-C_6H_4–CN, Ar_5 = *p*-C_6H_4–CN, Ar_3 = *p*-C_6H_4–CH_3). From 2.83 mmol of formazan **12b**: Yield = 0.18 g, 16%. mp = 169–171 °C. ^{1}H NMR (599.5 MHz, $CDCl_3$) δ 8.06 (d, $^3J_{HH}$ = 9 Hz, 4H, aryl C*H*), 7.96 (d, $^3J_{HH}$ = 8 Hz, 2H, aryl C*H*), 7.80 (d, $^3J_{HH}$ = 9 Hz, 4H, aryl C*H*), 7.32 (d, $^3J_{HH}$ = 8 Hz, 2H, aryl C*H*), 2.45 (s, 3H, CH_3). $^{13}C\{^1H\}$ NMR (100.6 MHz, $CDCl_3$): δ 146.7, 140.7, 133.3, 129.9, 129.7, 125.8, 123.9 (t, $^4J_{CF}$ = 3 Hz), 118.0, 113.5, 110.2, 21.6. ^{11}B NMR (128.3 MHz, $CDCl_3$): δ −0.7 (t, $^1J_{BF}$ = 29 Hz). ^{19}F NMR (376.1 Hz, $CDCl_3$): δ −141.8 (q, $^1J_{FB}$ = 29 Hz). FT-IR (KBr): 2949 (m), 2916 (m), 2847 (m), 2218 (s), 1650 (s), 1559 (m), 1507 (m), 1458 (m) cm^{-1}. UV–vis (toluene): λ_{max} = 548 nm (ε = 20 500 M^{-1} cm^{-1}). MS (EI, +ve mode): exact mass calculated for $[C_{22}H_{15}N_6BF_2]^+$: 412.14193; exact mass found: 412.14082; difference: −2.68 ppm. Anal. Calcd (%) for $C_{22}H_{15}N_6BF_2$: C, 64.10; H, 3.67; N, 20.39. Found: C, 64.38; H, 3.50; N, 20.08.

Formazanate BF_2 Complex 14c (Ar_1 = *p*-C_6H_4–OMe, Ar_5 = *p*-C_6H_4–OMe, Ar_3 = *p*-C_6H_4–CH_3). From 2.67 mmol of formazan **12c**: Yield = 0.83 g, 74%. mp = 186–188 °C. ^{1}H NMR (599.5 MHz, $CDCl_3$) δ 7.98 (d, $^3J_{HH}$ = 8 Hz, 2H, aryl C*H*), 7.86 (d, $^3J_{HH}$ = 9 Hz, 4H, aryl C*H*), 7.26 (d, $^3J_{HH}$ = 8 Hz, 2H, aryl C*H*), 6.96 (d, $^3J_{HH}$ = 9 Hz, 4H, aryl C*H*), 3.87 (s, 6H, OCH_3), 2.42 (s, 3H, CH_3). $^{13}C\{^1H\}$ NMR (100.6 MHz, $CDCl_3$): δ 160.8, 139.1, 137.8, 137.7, 131.4, 129.5, 125.5, 125.0 (t, $^4J_{CF}$ = 3 Hz), 114.4, 55.8, 21.5. ^{11}B NMR (128.3 MHz, $CDCl_3$): δ −0.7 (t, $^1J_{BF}$ = 29 Hz). ^{19}F NMR (376.1 Hz, $CDCl_3$): δ −145.7 (q, $^1J_{FB}$ = 29 Hz). FT-IR (KBr): 3025 (m), 2918 (m), 2794

dx.doi.org/10.1021/ic5016912 | Inorg. Chem. 2014, 53, 10585–10593

(m), 1653 (s), 1559 (m), 1508 (s), 1458 (m) cm^{-1}. UV−vis (toluene): λ_{max} = 552 nm (ε = 28 200 M^{-1} cm^{-1}). MS (EI, +ve mode): exact mass calculated for $[C_{22}H_{21}N_4O_2BF_2]^+$: 422.17256; exact mass found: 422.17452; difference: +4.63 ppm. Anal. Calcd (%) for $C_{22}H_{21}N_4O_2BF_2$: C, 62.58; H, 5.01; N, 13.27. Found: C, 62.52; H, 5.10; N, 12.56.

Formazanate BF_2 Complex 14d (Ar_1 = *p*-C_6H_4−CH_3, Ar_5 = *p*-C_6H_4−CH_3, Ar_3 = C_6H_5). From 3.04 mmol of formazan **12d**: Yield = 0.98 g, 84%. mp = 154−156 °C. ^{1}H NMR (599.5 MHz, $CDCl_3$) δ 8.10 (d, $^3J_{HH}$ = 7 Hz, 2H, aryl C*H*), 7.80 (d, $^3J_{HH}$ = 8 Hz, 4H, aryl C*H*), 7.46 (m, 2H, aryl C*H*), 7.27 (d, $^3J_{HH}$ = 8 Hz, 4H, aryl C*H*), 2.42 (s, 6H, CH_3). $^{13}C\{^1H\}$ NMR (100.6 MHz, $CDCl_3$): δ 141.9, 140.3, 134.0, 130.4, 129.8, 129.2, 128.8, 125.6, 123.4 (t, $^4J_{CF}$ = 3 Hz), 21.5. ^{11}B NMR (128.3 MHz, $CDCl_3$): δ −0.5 (t, $^1J_{BF}$ = 29 Hz). ^{19}F NMR (376.1 Hz, $CDCl_3$): δ −144.6 (q, $^1J_{FB}$ = 29 Hz). FT-IR (KBr): 2961 (m), 2873 (m), 1580 (s), 1500 (m), 1458 (m), 1267 (m) cm^{-1}. UV−vis (toluene): λ_{max} = 524 nm (ε = 30 300 M^{-1} cm^{-1}). MS (EI, +ve mode): exact mass calculated for $[C_{21}H_{19}N_4BF_2]^+$: 376.16707; exact mass found: 376.16705; difference: −0.26 ppm. Anal. Calcd (%) for $C_{21}H_{19}N_4BF_2$: C, 67.04; H, 5.09; N, 14.89. Found: C, 67.85; H, 5.35; N, 14.87.

Formazanate BF_2 Complex 14e (Ar_1 = *p*-C_6H_4−CH_3, Ar_5 = *p*-C_6H_4−CH_3, Ar_3 = *p*-C_6H_4−CN). From 2.83 mmol of formazan **12e**: Yield = 0.80 g, 70%. mp = 190−192 °C. ^{1}H NMR (599.5 MHz, $CDCl_3$) δ 8.23 (d, $^3J_{HH}$ = 8 Hz, 2H, aryl C*H*), 7.69 (d, $^3J_{HH}$ = 8 Hz, 2H, aryl C*H*), 7.58 (d, $^3J_{HH}$ = 8 Hz, 4H, aryl C*H*), 7.27 (d, $^3J_{HH}$ = 8 Hz, 4H, aryl C*H*), 2.41 (s, 6H, CH_3). $^{13}C\{^1H\}$ NMR (100.6 MHz, $CDCl_3$): δ 141.6, 140.9, 138.3, 132.6, 130.2, 129.9, 125.6, 123.3 (t, $^4J_{CF}$ = 2 Hz), 118.9, 112.2, 21.4. ^{11}B NMR (128.3 MHz, $CDCl_3$): δ 3.8 (t, $^1J_{BF}$ = 29 Hz). ^{19}F NMR (376.1 Hz, $CDCl_3$): δ −143.1 (q, $^1J_{FB}$ = 29 Hz). FT-IR (KBr): 3026 (m), 2914 (m), 2870 (m), 2222 (m), 1654 (s), 1559 (m), 1507 (s), 1458 (m) cm^{-1}. UV−vis (toluene): λ_{max} = 525 nm (ε = 25 300 M^{-1} cm^{-1}). MS (EI, +ve mode): exact mass calculated for $[C_{22}H_{18}N_5BF_2]^+$: 401.16232; exact mass found: 401.16103; difference: −3.16 ppm. Anal. Calcd (%) for $C_{22}H_{18}N_5BF_2$: C, 65.86; H, 4.52; N, 17.46. Found: C, 66.42; H, 4.63; N, 17.61.

Formazanate BF_2 Complex 14f (Ar_1 = *p*-C_6H_4−CH_3, Ar_5 = *p*-C_6H_4−CH_3, Ar_3 = *p*-C_6H_4−OMe). From 2.78 mmol of formazan **12f**: Yield = 0.81 g, 72%. mp = 166−168 °C. ^{1}H NMR (599.5 MHz, $CDCl_3$) δ 8.03 (d, $^3J_{HH}$ = 9 Hz, 2H, aryl C*H*), 7.78 (d, $^3J_{HH}$ = 9 Hz, 4H, aryl C*H*), 7.26 (d, $^3J_{HH}$ = 9 Hz, 4H, aryl C*H*), 6.99 (d, $^3J_{HH}$ = 9 Hz, 2H, aryl C*H*), 3.88 (s, 3H, OCH_3), 2.41 (s, 6H, CH_3). $^{13}C\{^1H\}$ NMR (100.6 MHz, $CDCl_3$): δ 160.6, 141.7, 141.7, 140.0, 129.7, 126.9, 126.5, 123.3 (t, $^4J_{CF}$ = 3 Hz), 114.1, 55.4, 21.4. ^{11}B NMR (128.3 MHz, $CDCl_3$): δ −0.6 (t, $^1J_{BF}$ = 29 Hz). ^{19}F NMR (376.1 Hz, $CDCl_3$): δ −145.8 (q, $^1J_{FB}$ = 29 Hz). FT-IR (KBr): 3035 (m), 3027 (m), 2997 (m), 2951 (m), 2916 (m), 2831 (m), 1605 (s), 1504 (m), 1455 (m) cm^{-1}. UV−vis (toluene): λ_{max} = 544 nm (ε = 25 800 M^{-1} cm^{-1}). MS (EI, +ve mode): exact mass calculated for $[C_{22}H_{21}N_4OBF_2]^+$: 406.17764; exact mass found: 406.17885; difference: +2.95 ppm. Anal. Calcd (%) for $C_{22}H_{21}N_4OBF_2$: C, 65.04; H, 5.21; N, 13.79. Found: C, 64.79; H, 5.22; N, 13.58.

Formazanate BF_2 Complex 14g (Ar_1 = *p*-C_6H_4−CN, Ar_5 = *p*-C_6H_4−OMe, Ar_3 = *p*-C_6H_4−CH_3). From 2.70 mmol of formazan **12g**: Yield = 0.82 g, 73%. mp = 151−153 °C. ^{1}H NMR (599.5 MHz, $CDCl_3$) δ 7.98 (m, 6H, aryl C*H*), 7.72 (d, $^3J_{HH}$ = 9 Hz, 2H, aryl C*H*), 7.29 (d, $^3J_{HH}$ = 8 Hz, 2H, aryl C*H*), 7.01 (d, $^3J_{HH}$ = 9 Hz, 2H, aryl C*H*), 3.90 (s, 3H, OCH_3), 2.43 (s, 3H, CH_3). $^{13}C\{^1H\}$ NMR (100.6 MHz, $CDCl_3$): δ 162.3, 147.4, 139.9, 137.7, 133.1, 130.7, 129.7, 125.7 (t, $^4J_{CF}$ = 3 Hz), 125.7, 123.1 (t, $^4J_{CF}$ = 3 Hz), 118.6, 114.9, 114.8, 111.3, 55.9, 21.5. ^{11}B NMR (128.3 MHz, $CDCl_3$): δ −0.6 (t, $^1J_{BF}$ = 29 Hz). ^{19}F NMR (376.1 Hz, $CDCl_3$): δ −142.9 (q, $^1J_{FB}$ = 29 Hz). FT-IR (KBr): 3004 (m), 2985 (m), 2910 (m), 2834 (m), 2222 (s), 1596 (s), 1505 (s), 1295 (m), 1254 (s), 1170 (m) cm^{-1}. UV−vis (toluene): λ_{max} = 561 nm (ε = 24 400 M^{-1} cm^{-1}). MS (EI, +ve mode): exact mass calculated for $[C_{22}H_{18}N_5OBF_2]^+$: 417.15725; exact mass found: 417.16088; difference: +8.70 ppm. Anal. Calcd (%) for $C_{22}H_{18}N_5OBF_2$: C, 63.33; H, 4.35; N, 16.79 Found: C, 63.40; H, 4.43; N, 15.99.

Formazanate BF_2 Complex 14h (Ar_1 = *p*-C_6H_4−CH_3, Ar_5 = *p*-C_6H_4−CN, Ar_3 = *p*-C_6H_4−OMe). From 2.70 mmol of formazan **12h**: Yield = 1.03 g, 92%. mp = 154−156 °C. ^{1}H NMR (599.5 MHz, $CDCl_3$) δ 8.02 (d, $^3J_{HH}$ = 9 Hz, 2H, aryl C*H*), 7.99 (d, $^3J_{HH}$ = 8 Hz, 2H, aryl C*H*), 7.84 (d, $^3J_{HH}$ = 8 Hz, 2H, aryl C*H*), 7.74 (d, $^3J_{HH}$ = 9 Hz, 2H, aryl C*H*), 7.31 (d, $^3J_{HH}$ = 8 Hz, 2H, aryl C*H*), 7.01 (d, $^3J_{HH}$ = 9 Hz, 2H, aryl C*H*), 3.89 (s, 3H, OCH_3), 2.44 (s, 3H, CH_3). $^{13}C\{^1H\}$ NMR (100.6 MHz, $CDCl_3$): δ 161.2, 147.4, 142.2, 141.9, 133.2, 130.2, 127.3, 125.9, 123.9 (t, $^4J_{CF}$ = 2 Hz), 123.4 (t, $^4J_{CF}$ = 3 Hz), 118.6, 114.5, 111.8, 111.1, 55.7, 21.7. ^{11}B NMR (128.3 MHz, $CDCl_3$): δ −0.7 (t, $^1J_{BF}$ = 29 Hz). ^{19}F NMR (376.1 Hz, $CDCl_3$): δ −145.7 (q, $^1J_{FB}$ = 29 Hz). FT-IR (KBr): 3035 (m), 3026 (m), 2998 (m), 2931 (m), 2835 (m), 2227 (s), 1603 (s), 1509 (s), 130 (m), 1248 (s), 1170 (m) cm^{-1}. UV−vis (toluene): λ_{max} = 554 nm (ε = 21 500 M^{-1} cm^{-1}). MS (EI, +ve mode): exact mass calculated for $[C_{22}H_{18}N_5OBF_2]^+$: 417.15725; exact mass found: 417.15788; difference: +1.50 ppm. Anal. Calcd (%) for $C_{22}H_{18}N_5OBF_2$: C, 63.33; H, 4.35; N, 16.79. Found: C, 63.35; H, 4.47; N, 15.98.

Formazanate BF_2 Complex 14i (Ar_1 = *p*-C_6H_4−OMe, Ar_5 = *p*-C_6H_4−CH_3, Ar_3 = *p*-C_6H_4−CN). From 2.70 mmol of formazan **12i**: Yield = 0.62 g, 55%. mp = 172−174 °C. ^{1}H NMR (599.5 MHz, $CDCl_3$) δ 8.21 (d, $^3J_{HH}$ = 8 Hz, 2H, aryl C*H*), 7.89 (d, $^3J_{HH}$ = 9 Hz, 2H, aryl C*H*), 7.78 (d, $^3J_{HH}$ = 8 Hz, 2H, aryl C*H*), 7.74 (d, $^3J_{HH}$ = 8 Hz, 2H, aryl C*H*), 7.28 (d, $^3J_{HH}$ = 8 Hz, 2H, aryl C*H*), 6.99 (d, $^3J_{HH}$ = 9 Hz, 2H, aryl C*H*), 3.89 (s, 3H, OCH_3), 2.43 (s, 3H, CH_3). $^{13}C\{^1H\}$ NMR (100.6 MHz, $CDCl_3$): δ 161.5, 140.7, 140.6, 138.5, 137.5, 132.7, 130.0, 125.7, 125.3 (t, $^4J_{CF}$ = 3 Hz), 125.3, 123.3 (t, $^4J_{CF}$ = 3 Hz), 119.0, 114.7, 112.3, 55.9, 21.5. ^{11}B NMR (128.3 MHz, $CDCl_3$): δ −0.6 (t, $^1J_{BF}$ = 29 Hz). ^{19}F NMR (376.1 Hz, $CDCl_3$): δ −143.4 (q, $^1J_{FB}$ = 29 Hz). FT-IR (KBr): 3035 (m), 3001 (m), 2997 (m), 2911 (m), 2835 (m), 2227 (m), 1599 (s), 1507 (s), 1318 (m), 1256 (s), 1168 (s) cm^{-1}. UV−vis (toluene): λ_{max} = 541 nm (ε = 25 100 M^{-1} cm^{-1}). MS (EI, +ve mode): exact mass calculated for $[C_{22}H_{18}N_5OBF_2]^+$: 417.15725; exact mass found: 417.15829; difference: +2.50 ppm. Anal. Calcd (%) for $C_{22}H_{18}N_5OBF_2$: C, 63.33; H, 4.35; N, 16.79. Found: C, 64.33; H, 4.43; N, 16.76.

■ ASSOCIATED CONTENT

Ⓢ Supporting Information

^{1}H and ^{13}C NMR spectra, UV-vis absorption and emission spectra, and cyclic voltammograms. This material is available free of charge via the Internet at http://pubs.acs.org.

■ AUTHOR INFORMATION

Corresponding Author

*E-mail: joe.gilroy@uwo.ca. Phone: +1-519-661-2111 ext. 81561. Fax: +1-519-661-3022.

Notes

The authors declare no competing financial interest.

■ REFERENCES

(1) For example: (a) Belcher, W. J.; Hodgson, M. C.; Sumida, K.; Torvisco, A.; Ruhlandt-Senge, K.; Ware, D. C.; Boyd, P. D. W.; Brothers, P. J. *Dalton Trans.* **2008**, 1602−1614. (b) Cheng, F.; Jäkle, F. *Chem. Commun.* **2010**, *46*, 3717−3719. (c) Fischer, G. M.; Daltrozzo, E.; Zumbusch, A. *Angew. Chem., Int. Ed.* **2011**, *50*, 1406−1409. (d) Vogels, C. M.; Westcott, S. A. *Chem. Soc. Rev.* **2011**, *40*, 1446−1458. (e) Roacho, R. I.; Metta-Magaña, A.; Portillo, M. M.; Peña-Cabrera, E.; Pannell, K. H. *J. Org. Chem.* **2013**, *78*, 4245−4250. (f) Bonnier, C.; Machin, D. D.; Abdi, O.; Koivisto, B. D. *Org. Biomol. Chem.* **2013**, *11*, 3756−3760. (g) Frath, D.; Poirel, A.; Ulrich, G.; De Nicola, A.; Ziessel, R. *Chem. Commun.* **2013**, *49*, 4908−4910. (h) Lu, J.-S.; Ko, S.-B.; Walters, N. R.; Kang, Y.; Sauriol, F.; Wang, S. *Angew. Chem., Int. Ed.* **2013**, *52*, 4544−4548. (i) Firinci, E.; Bates, J. I.; Riddlestone, I. M.; Phillips, N.; Aldridge, S. *Chem. Commun.* **2013**, *49*, 1509−1511. (j) Frath, D.; Massue, J.; Ulrich, G.; Ziessel, R. *Angew. Chem., Int. Ed.* **2014**, *53*, 2290−2310.

(2) Reviews: (a) Loudet, A.; Burgess, K. *Chem. Rev.* **2007**, *107*, 4891−4932. (b) Ulrich, G.; Ziessel, R.; Harriman, A. *Angew. Chem., Int. Ed.* **2008**, *47*, 1184−1201. (c) Boens, N.; Leen, V.; Dehaen, W. *Chem. Soc. Rev.* **2012**, *41*, 1130−1172.
(3) (a) Qian, B.; Baek, S. W.; Smith, M. R., III *Polyhedron* **1999**, *18*, 2405−2414. (b) Macedo, F. P.; Gwengo, C.; Lindeman, S. V.; Smith, M. D.; Gardinier, J. R. *Eur. J. Inorg. Chem.* **2008**, 3200−3211. (c) Barbon, S. M.; Staroverov, V. N.; Boyle, P. D.; Gilroy, J. B. *Dalton Trans.* **2014**, *43*, 240−250.
(4) Araneda, J. F.; Piers, W. E.; Heyne, B.; Parvez, M.; McDonald, R. *Angew. Chem., Int. Ed.* **2011**, *50*, 12214−12217.
(5) (a) Ren, Y.; Liu, X.; Gao, W.; Xia, H.; Ye, L.; Mu, Y. *Eur. J. Inorg. Chem.* **2007**, 1808−1814. (b) Liu, X.; Ren, Y.; Xia, H.; Fan, X.; Mu, Y. *Inorg. Chim. Acta* **2010**, *363*, 1441−1447.
(6) Kubota, Y.; Tsuzuki, T.; Funabiki, K.; Ebihara, M.; Matsui, M. *Org. Lett.* **2010**, *12*, 4010−4013.
(7) (a) Nawn, G.; Waldie, K. M.; Oakley, S. R.; Peters, B. D.; Mandel, D.; Patrick, B. O.; McDonad, R.; Hicks, R. G. *Inorg. Chem.* **2011**, *50*, 9826−9837. (b) Nawn, G.; Oakley, S. R.; Majewski, M. B.; McDonald, R.; Patrick, B. O.; Hicks, R. G. *Chem. Sci.* **2013**, *4*, 612−621.
(8) For example: (a) Hudnall, T. W.; Gabbaï, F. P. *Chem. Commun.* **2008**, 4596−4597. (b) Lazarides, T.; McCormick, T. M.; Wilson, K. C.; Lee, S.; McCamant, D. W.; Eisenberg, R. *J. Am. Chem. Soc.* **2010**, *133*, 350−364. (c) Bozdemir, O. A.; Erbas-Cakmak, S.; Ekiz, O. O.; Dana, A.; Akkaya, E. U. *Angew. Chem., Int. Ed.* **2011**, *50*, 10907−10912. (d) Zhang, C.; Zhao, J.; Wu, S.; Wang, Z.; Wu, W.; Ma, J.; Guo, S.; Huang, L. *J. Am. Chem. Soc.* **2013**, *135*, 10566−10578. (e) Carlson, J. C. T.; Meimetis, L. G.; Hilderbrand, S. A.; Weissleder, R. *Angew. Chem., Int. Ed.* **2013**, *52*, 6917−6920. (f) Manjare, S. T.; Kim, J.; Lee, Y.; Churchill, D. G. *Org. Lett.* **2013**, *16*, 520−523.
(9) Reviews: (a) Nineham, A. W. *Chem. Rev.* **1955**, *55*, 355−483. (b) Sigeiken, G. I.; Lipunova, G. N.; Pervova, I. G. *Russ. Chem. Rev.* **2006**, *75*, 885−900.
(10) (a) Gök, Y. *Dyes Pigm.* **1989**, *11*, 101−107. (b) Gök, Y.; Şentürk, H. B. *Dyes Pigm.* **1991**, *15*, 279−287. (c) Zhang, Y.; Liu, D. *Dyes Pigm.* **1995**, *29*, 57−63. (d) Szymczyk, M.; El-Shafei, A.; Freeman, H. S. *Dyes Pigm.* **2007**, *72*, 8−15.
(11) For example: (a) Weislow, O. S.; Kiser, R.; Fine, D. L.; Bader, J.; Shoemaker, R. H.; Boyd, M. R. *J. Natl. Cancer Inst.* **1989**, *81*, 577−586. (b) Abou-Elenien, G. M. *J. Electroanal. Chem.* **1994**, *375*, 301−305. (c) Goodwin, C. J.; Holt, S. J.; Downes, S.; Marshall, N. J. *J. Immunol. Methods* **1995**, *179*, 95−103. (d) Gruden, C. L.; Fevig, S.; Abu-Dalo, M.; Hernandez, M. *J. Microbiol. Methods* **2003**, *52*, 59−68. (e) Frederiks, W. M.; van Marle, J.; van Oven, C.; Comin-Anduix, B.; Cascante, M. *J. Histochem. Cytochem.* **2006**, *54*, 47−52.
(12) For example: (a) Hunter, L.; Roberts, C. B. *J. Chem. Soc.* **1941**, 823−826. (b) Irving, H.; Gill, J. B.; Cross, W. R. *J. Chem. Soc.* **1960**, 2087−2095. (c) Siedle, A. R.; Pignolet, L. H. *Inorg. Chem.* **1980**, *19*, 2052−2056. (d) Jameson, G. B.; Muster, A.; Robinson, S. D.; Wingfield, J. N.; Ibers, J. A. *Inorg. Chem.* **1981**, *20*, 2448−2456. (e) Brown, D. A.; Bögge, H.; Lipunova, G. N.; Müller, A.; Plass, W.; Walsh, K. G. *Inorg. Chim. Acta* **1998**, *280*, 30−38. (f) Gilroy, J. B.; Ferguson, M. J.; McDonald, R.; Patrick, B. O.; Hicks, R. G. *Chem. Commun.* **2007**, 126−128. (g) Gilroy, J. B.; Ferguson, M. J.; McDonald, R.; Hicks, R. G. *Inorg. Chim. Acta* **2008**, *361*, 3388−3393. (h) Gilroy, J. B.; Patrick, B. O.; McDonald, R.; Hicks, R. G. *Inorg. Chem.* **2008**, *47*, 1287−1294. (i) Hong, S.; Hill, L. M. R.; Gupta, A. K.; Naab, B. D.; Gilroy, J. B.; Hicks, R. G.; Cramer, C. J.; Tolman, W. B. *Inorg. Chem.* **2009**, *48*, 4514−4523. (j) Hong, S.; Gupta, A. K.; Tolman, W. B. *Inorg. Chem.* **2009**, *48*, 6323−6325.
(13) Chang, M.-C.; Dann, T.; Day, D. P.; Lutz, M.; Wildgoose, G. G.; Otten, E. *Angew. Chem., Int. Ed.* **2014**, *53*, 4118−4122.
(14) Chang, M.-C.; Otten, E. *Chem. Commun.* **2014**, *50*, 7431−7433.
(15) Barbon, S. M.; Reinkeluers, P. A.; Price, J. T.; Staroverov, V. N.; Gilroy, J. B. *Chem.—Eur. J.* **2014**, *20*, 11340−11344.
(16) (a) Katritzky, A. A.; Belyakov, S. A.; Cheng, D.; Durst, H. D. *Synthesis* **1995**, *1995*, 577−581. (b) Gilroy, J. B.; McKinnon, S. D. J.; Koivisto, B. D.; Hicks, R. G. *Org. Lett.* **2007**, *9*, 4837−4840.
(17) This reaction was repeated several times; in each case the major component of the reaction mixture was unreacted formazan **12b**.
(18) *CRC Handbook of Chemistry and Physics;* CRC Press: Boca Raton, FL, 2012.
(19) Fery-Forgues, S.; Lavabre, D. *J. Chem. Educ.* **1999**, *76*, 1260−1264.
(20) Suzuki, K.; Kobayashi, A.; Kaneko, S.; Takehira, K.; Yoshihara, T.; Ishida, H.; Shiina, Y.; Oishi, S.; Tobita, S. *Phys. Chem. Chem. Phys.* **2009**, *11*, 9850−9860.
(21) Gilroy, J. B.; McKinnon, S. D. J.; Kennepohl, P.; Zsombor, M. S.; Ferguson, M. J.; Thompson, L. K.; Hicks, R. G. *J. Org. Chem.* **2007**, *72*, 8062−8069.
(22) For example: (a) Ziessel, R.; Retailleau, P.; Elliott, K. J.; Harriman, A. *Chem.—Eur. J.* **2009**, *15*, 10369−10374. (b) Didier, P.; Ulrich, G.; Mély, Y.; Ziessel, R. *Org. Biomol. Chem.* **2009**, *7*, 3639−3642. (c) Collado, D.; Casado, J.; Rodríguez González, S.; López Navarrete, J. T.; Suau, R.; Perez-Inestrosa, E.; Pappenfus, T. M.; Raposo, M. M. M. *Chem.—Eur. J.* **2011**, *17*, 498−507. (d) Niu, S.; Ulrich, G.; Retailleau, P.; Ziessel, R. *Tetrahedron Lett.* **2011**, *52*, 4848−4853. (e) Shi, W.-J.; Lo, P.-C.; Singh, A.; Ledoux-Rak, I.; Ng, D. K. P. *Tetrahedron* **2012**, *68*, 8712−8718. (f) Ulrich, G.; Barsella, A.; Boeglin, A.; Niu, S.; Ziessel, R. *ChemPhysChem* **2014**, *15*, 2693−2700.
(23) For example: (a) Zhou, Y.; Xiao, Y.; Chi, S.; Qian, X. *Org. Lett.* **2008**, *10*, 633−636. (b) Wu, Y.-Y.; Chen, Y.; Gou, G.-Z.; Mu, W.-H.; Lv, X.-J.; Du, M.-L.; Fu, W.-F. *Org. Lett.* **2012**, *14*, 5226−5229. (c) D'Aléo, A.; Gachet, D.; Heresanu, V.; Giorgi, M.; Fages, F. *Chem.—Eur. J.* **2012**, *18*, 12764−12772. (d) D'Aléo, A.; Fages, F. *Photochem. Photobiol. Sci.* **2013**, *12*, 500−510.
(24) Lakowicz, J. R. *Principles of Fluorescence Spectroscopy,* 3rd ed.; Springer: New York, 2006.
(25) (a) Jiao, L.; Yu, C.; Liu, M.; Wu, Y.; Cong, K.; Meng, T.; Wang, Y.; Hao, E. *J. Org. Chem.* **2010**, *75*, 6035−6038. (b) Sobenina, L. N.; Vasil'tsov, A. M.; Petrova, O. V.; Petrushenko, K. B.; Ushakov, I. A.; Clavier, G.; Meallet-Renault, R.; Mikhaleva, A. I.; Trofimov, B. A. *Org. Lett.* **2011**, *13*, 2524−2527. (c) Leen, V.; Miscoria, D.; Yin, S.; Filarowski, A.; Molisho Ngongo, J.; Van der Auweraer, M.; Boens, N.; Dehaen, W. *J. Org. Chem.* **2011**, *76*, 8168−8176.
(26) Bruker-Nonius, *SAINT,* version 2013.8; Bruker-AXS: Madison, WI, 2013.
(27) Bruker-Nonius, *SADABS,* version 2012.1; Bruker-AXS: Madison, WI, 2012.
(28) Bruker-AXS, *XS,* version 2013.12; Bruker-AXS: Madison, WI, 2013.
(29) Sheldrick, G. M. *Acta Crystallogr.* **2008**, *A64*, 112−122.
(30) Spek, A. L. *Acta Crystallogr.* **1990**, *A46*, 194−201.

■ NOTE ADDED AFTER ASAP PUBLICATION

This paper was published on the Web on September 16, 2014, with minor text errors throughout the paper. The corrected version was reposted on September 24, 2014.